Quadrature phase-shift error analysis using a homodyne laser interferometer

Peter Gregorčič,* Tomaž Požar, and Janez Možina

Faculty of Mechanical Engineering, University of Ljubljana, Aškerčeva 6, 1000 Ljubljana, Slovenia
*peter.gregorcic@fs.uni-lj.si

Abstract: The influence of quadrature phase shift on the measured displacement error was experimentally investigated using a two-detector polarizing homodyne laser interferometer with a quadrature detection system. Common nonlinearities, including the phase-shift error, were determined and effectively corrected by a robust data-processing algorithm. The measured phase-shift error perfectly agrees with the theoretically determined phase-shift error region. This error is systematic, periodic and severely asymmetrical around the nominal displacement value. The main results presented in this paper can also be used to assess and correct the detector errors of other interferometric and non-interferometric displacement-measuring devices based on phase-quadrature detection.

References and links

1. N. Bobroff, "Recent advances in displacement measuring interferometry," Meas. Sci. Technol. **4**(9), 907–926 (1993).
2. R. Reibold, and W. Molkenstruck, "Laser interferometric measurement and computerized evaluation of ultrasonic displacements," Acustica **49**, 205–211 (1981).
3. V. Greco, G. Molesini, and F. Quercioli, "Accurate polarization interferometer," Rev. Sci. Instrum. **66**(7), 3729–3734 (1995).
4. T. Keem, S. Gonda, I. Misumi, Q. Huang, and T. Kurosawa, "Removing nonlinearity of a homodyne interferometer by adjusting the gains of its quadrature detector systems," Appl. Opt. **43**(12), 2443–2448 (2004).
5. M. Novak, J. Millerd, N. Brock, M. North-Morris, J. Hayes, and J. Wyant, "Analysis of a micropolarizer array-based simultaneous phase-shifting interferometer," Appl. Opt. **44**(32), 6861–6868 (2005).
6. L. M. Sanchez-Brea, and T. Morlanes, "Metrological errors in optical encoders," Meas. Sci. Technol. **19**(11), 115104 (2008).
7. T. Požar, R. Petkovšek, and J. Možina, "Dispersion of an optodynamic wave during its multiple transitions in a rod," Appl. Phys. Lett. **92**(23), 234101–234103 (2008).
8. G. L. Dai, F. Pohlenz, H. U. Danzebrink, K. Hasche, and G. Wilkening, "Improving the performance of interferometers in metrological scanning probe microscopes," Meas. Sci. Technol. **15**(2), 444–450 (2004).
9. N.-I. Toto-Arellano, G. Rodriguez-Zurita, C. Meneses-Fabian, and J. F. Vazquez-Castillo, "Phase shifts in the Fourier spectra of phase gratings and phase grids: an application for one-shot phase-shifting interferometry," Opt. Express **16**(23), 19330–19341 (2008).
10. P. L. M. Heydemann, "Determination and correction of quadrature fringe measurement errors in interferometers," Appl. Opt. **20**(19), 3382–3384 (1981).
11. C.-M. Wu, and C.-S. Su, "Nonlinearity in measurements of length by optical interferometry," Meas. Sci. Technol. **7**(1), 62–68 (1996).
12. T. Usuda, and T. Kurosawa, "Calibration methods for vibration transducers and their uncertainties," Metrologia **36**(4), 375–383 (1999).
13. K. P. Birch, "Optical fringe subdivision with nanometric accuracy," Precis. Eng. **12**(4), 195–198 (1990).
14. C.-M. Wu, C.-S. Su, and G.-S. Peng, "Correction of nonlinearity in one-frequency optical interferometry," Meas. Sci. Technol. **7**(4), 520–524 (1996).
15. T. Eom, J. Kim, and K. Jeong, "The dynamic compensation of nonlinearity in a homodyne laser interferometer," Meas. Sci. Technol. **12**(10), 1734–1738 (2001).
16. J.-A. Kim, J. W. Kim, C.-S. Kang, T. B. Eom, and J. Ahn, "A digital signal processing module for real-time compensation of nonlinearity in a homodyne interferometer using a field-programmable gate array," Meas. Sci. Technol. **20**(1), 017003 (2009).
17. C. B. Scruby and L. E. Drain, Laser Ultrasonics: Techniques and Applications, (Adam Hilger, Bristol, 1990).

18. I. Dániel, "Advanced successive phase unwrapping algorithm for quadrature output Michelson interferometers," Measurement **37**(2), 95–102 (2005).
19. M. Pisani, "Multiple reflection Michelson interferometer with picometer resolution," Opt. Express **16**(26), 21558–21563 (2008).

1. Introduction

Detection methods based on two or more signals in phase quadrature allow nano-resolution and high-dynamic-range displacement measurements with a constant sensitivity [1]. The quadrature signals can be obtained in various laser interferometers [2–5] as well as in other types of displacement-measuring systems, for example, optical encoders [6]. A great interest for accurate displacement measurements with sub-fringe accuracy arises from many interesting applications, such as: measurements of high-amplitude ultrasound on stationary and moving objects [7], metrology analysis including scanning probe microscopes [8], and applications based on phase-shifting interferometry [5,9].

The precision and accuracy of a displacement measured with quadrature-detection systems are limited by a set of errors [1,10,11] that generally arise from mechanical, optical, and electric sources. When the phase shift between the detected signals deviates from the ideal 90°, the phase-unwrapping procedure [12] generates an error in the displacement. To analyze this error experimentally, other errors (e.g., unequal gains, zero offsets, deviations from the harmonic signal shape, etc.) need to be eliminated or corrected. This can be most conveniently realized in a homodyne quadrature laser interferometer (HQLI) with two orthogonally polarized signals [2].

In a HQLI, the phase shift can be continuously varied by rotating a wave plate. However, the rotation of the wave plate also produces unequal signal amplitudes and different zero offsets, both of which can be corrected with the appropriate signal processing. Additionally, in a HQLI, the deviations from the harmonic signal shape [6] are minimal [11], since the intensities on the photodiodes vary harmonically due to the inherent physical properties of the interferometer.

The three commonly encountered systematic nonlinearities of a detector—unequal AC amplitudes, DC offsets, and quadrature phase-shift error—are typically all determined and corrected together using a traditional elliptical fitting technique based on a least-squares method [10,13,14]. Because the main aim of our study was to present the influence of quadrature phase shift on the measured displacement error, we separated the phase-shift error from the other two errors with specially developed software based on the processing algorithm described in this paper. Moreover, the separation of errors reduces the number of least-squares fitting parameters from four (two DC offsets, ratio of AC amplitudes, and phase-shift) to only one, i.e., phase-shift. Our software makes it possible to acquire the raw signals, process the data, and also to estimate and correct the common detector errors. Since the data processing includes only one least-squares fitting parameter it proved more robust and faster than fitting the ellipse in the traditional way. When a real-time correction of the nonlinearities is needed, the data processing described here can be implemented in a suitable digital or analogue signal-processing module [15,16].

This paper investigates the displacement error due to the lack of quadrature with a two-detector homodyne laser interferometer. The performance of the HQLI operating with an arbitrary phase shift is described using Jones calculus. We present robust data processing to obtain the error-corrected displacement, where the phase-shift error is separated from the other nonlinearities. The quadrature phase-shift error is measured, the theoretical error region is determined and the error is qualitatively and quantitatively evaluated. The main results are discussed and the applicability for other quadrature-detection systems is proposed.

2. Homodyne quadrature laser interferometer

There are two basic variants of the HQLI with regard to the number of detected signals. A balanced scheme with four detectors uses all the available laser light, is insensitive to laser output power drifts, has twice the number of detectors, compared to the two-detector variant,

and more than twice the number of optical components [3,17]. However, several errors in the detected displacement may arise from misaligned or imperfect optical components [11]. With this in mind we realized an experimental two-detector HQLI, trying to reduce the possible errors (polarization-mixing cross talk [11,14], ghost images, waveform distortions, etc.) that originate from the imperfect optical components and contribute to the final error in the measured displacement. We set such a homodyne quadrature interferometer so that the phase shift can be controlled only by the rotation of the wave plate, except for the constant contribution of the polarization-sensitive light reflections at the beamsplitter explained in section 4. Compared to the laser-power insensitive four-detector scheme, the two-detector variant needs an additional photo-detector [18] or a stabilized laser source [1]; we employed the latter. A detailed comparison between the four- and two-detector scheme can be found elsewhere [3].
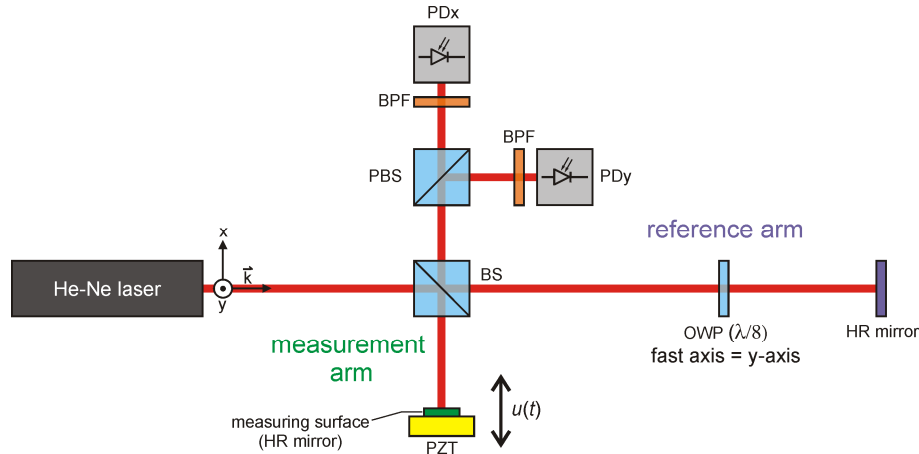

Fig. 1. Schematic top view of the HQLI. The exiting light from the stabilized He-Ne laser is linearly polarized at $45°$ in the x-y plane. The beamsplitter (BS) evenly splits the beam into the reference and measurement arms. The octadic-wave plate (OWP) and high-reflectivity (HR) mirror are placed in the reference arm. The HR mirror in the measurement arm is driven by a piezoelectric transducer (PZT). The polarizing beamsplitter (PBS) transmits the x-polarization and reflects the y-polarization. An optically narrow band-pass filter (BPF) is placed before the photodiodes labeled PDx and PDy.

The top view of the HQLI setup is schematically illustrated in Fig. 1. The cylindrical head of the polarized and stabilized He-Ne laser ($\lambda = 632.8$ nm; amplitude stability over 1 min < 0.2% and amplitude noise (0 – 10 MHz) < 0.2%) is rotated so that the linearly polarized beam exiting the laser forms a $45°$ angle with respect to the plane of the optical table (x-plane). This polarization can be decomposed into two orthogonal polarizations with equal intensities, one in the plane of the paper (x-axis) and the other perpendicular to it (y-axis). The beamsplitter (BS) evenly splits the beam into the reference and measurement arms. The first transition through the octadic-wave plate (OWP), which is placed in the reference arm, gives rise to the $45°$ ($\lambda/8$) phase difference between the orthogonal polarizations. The beam is then reflected from a high-reflectivity (HR) mirror and another $45°$ are added on the returning passage through the OWP. The orthogonal polarizations in the measurement arm experience an equal phase shift $\delta(u)$ due to the movement of the measuring surface, which is driven by a piezoelectric transducer (PZT). The light in phase opposition is not detected since it returns towards the laser. The PBS transmits the x-polarization and reflects the y-polarization. An optically narrow band-pass filter (BPF) is placed before the photodiodes labeled PDx and PDy to attenuate the scattered light at different wavelengths.

The operation of a HQLI with two orthogonally polarized signals with an arbitrary phase shift can be conveniently described using Jones calculus [3,4]. Each optical component in the interferometer is represented by a matrix. Multiplying the matrices to the left mathematically modifies the electric field vector. This corresponds to the light passing through the optical

components. Normalizing the electric field amplitude to unity, the electric field vector of the linearly polarized light **E** and the ideal optical components found in the HQLI can be written as:

$$\mathbf{E}(45°) = \frac{1}{\sqrt{2}}\begin{bmatrix} 1 \\ 1 \end{bmatrix}, \quad bs = \frac{1}{\sqrt{2}}\begin{bmatrix} 1 & 0 \\ 0 & 1 \end{bmatrix}, \quad pbs_x = \begin{bmatrix} 1 & 0 \\ 0 & 0 \end{bmatrix}, \quad pbs_y = \begin{bmatrix} 0 & 0 \\ 0 & 1 \end{bmatrix},$$

$$opd = e^{i\delta}\begin{bmatrix} 1 & 0 \\ 0 & 1 \end{bmatrix}, \quad owp(\varphi) = \begin{bmatrix} \cos\dfrac{\pi}{8} - i\sin\dfrac{\pi}{8}\cos 2\varphi & -i\sin\dfrac{\pi}{8}\sin 2\varphi \\[2mm] -i\sin\dfrac{\pi}{8}\sin 2\varphi & \cos\dfrac{\pi}{8} + i\sin\dfrac{\pi}{8}\cos 2\varphi \end{bmatrix}.$$

Here, bs corresponds to the 50%-50% BS, pbs_x to the PBS's transmitted output with the polarization in the x-plane, pbs_y to the reflected output with the polarization in the perpendicular direction (y-plane), opd is the phase factor that accounts for the optical phase difference between the two arms arising from the displacement of the measuring surface, and owp is an octadic-wave plate that can be rotated by an arbitrary angle φ, measured from the y-plane to the OWP's fast axis.

Two interfering beams with polarizations in the x-plane, one from the reference arm and the other from the measurement arm, reach the photodiode PDx. Similarly, the perpendicular polarizations coming from both arms illuminate the photodiode PDy. Ideally, the interference signals on the photodiodes are shifted by 90°, which can be achieved with a properly rotated OWP. The measured displacement u is encoded in the phase $\delta(u) = 4\pi u/\lambda$, where λ is the wavelength of the interferometric laser. The electric fields arising from the reference (index r) and the measurement (index m) arms can be calculated using the Jones matrix formalism as:

$$\mathbf{E}_{rx,ry} = pbs_{x,y} \cdot bs \cdot owp(\varphi) \cdot owp(\varphi) \cdot bs \cdot \mathbf{E}(45°),$$

$$\mathbf{E}_{mx,my} = pbs_{x,y} \cdot bs \cdot opd \cdot bs \cdot \mathbf{E}(45°).$$

The interference of the two beams on the PDx and PDy is calculated using

$$I_{x,y} = I_0 (\mathbf{E}_{rx,ry} + \mathbf{E}_{mx,my})^\dagger \cdot (\mathbf{E}_{rx,ry} + \mathbf{E}_{mx,my})$$

and this yields the corresponding intensities, I_x and I_y, as a function of the optical phase difference δ and the angle of the OWP rotation φ. The dagger denotes the conjugate transpose and I_0 stands for the laser output intensity. The intensities on the photodiodes are:

$$I_x(\delta,\varphi) = \frac{I_0}{16}\left(4 + \sin 4\varphi + 2\sqrt{2}\left(\cos\delta - \sin\delta(\cos 2\varphi + \sin 2\varphi)\right)\right), \qquad (1a)$$

$$I_y(\delta,\varphi) = \frac{I_0}{16}\left(4 - \sin 4\varphi + 2\sqrt{2}\left(\cos\delta + \sin\delta(\cos 2\varphi - \sin 2\varphi)\right)\right). \qquad (1b)$$

Under ideal conditions, when the fast axis of the OWP is perpendicular to the x-plane, the signals are in phase quadrature:

$$I_x(\delta - 45°, 0°) = \frac{I_0}{4}(1 + \cos\delta) \quad \text{and} \quad I_y(\delta - 45°, 0°) = \frac{I_0}{4}(1 + \sin\delta). \qquad (2)$$

The influence of φ on the detected displacement will be discussed later. The displacement of the measuring surface along the line of the laser beam can be derived from the ideal quadrature signals I_x and I_y (Eq. (2)) by subtracting the DC offset as:

$$u(t) = \frac{\lambda}{4\pi} \left(\arctan \frac{I_y - I_0/4}{I_x - I_0/4} + m\pi \right), \quad m = 0, \pm 1, \pm 2, \ldots . \tag{3}$$

The integer m has to be chosen correctly so that the function $u(t)$ becomes continuous.

3. Signal processing

The phase-modulated intensities on the photodiodes, I_x and I_y, are detected as the photodiode output signals, $V_x(t)$ and $V_y(t)$, which were equidistantly sampled by a 500-MHz oscilloscope with a sampling capacity of 2 MS per channel. The sampling is limited either by the oscilloscope's sampling rate or by the frequency response of the photodiodes. Assuming that the acquired (raw) signals take the following distorted form

$$V_{x,y}(u(t)) = V_{x0,y0} \cos\left(\frac{4\pi}{\lambda} u(t) - \delta_{x,y} \right) + V_{xoff,yoff} \tag{4}$$

they have to be corrected so that the phase unwrapping (Eq. (3)) yields an accurate displacement. Here, $V_{x0,y0}$ stands for the AC amplitudes of the detected voltage, $\delta_{x,y}$ are the corresponding initial phases and $V_{xoff,yoff}$ are the DC offsets. $V_{x0,y0}$ and $V_{xoff,yoff}$ are constants, because we ensured a highly constant laser output power within the acquisition time. A few error sources influence only a single parameter in Eq. (4), while, for example, rotating the OWP contributes to a change in all the parameters in Eq. (4), as described by Eqs. (1).

Typical raw signals, acquired from photodiodes, when the piezoelectric transducer (PZT) vibrating with a frequency $f = 100$ Hz harmonically moves the measuring HR mirror by an amplitude $A = 270$ nm are shown in Fig. 2(a). After the raw signals were acquired from photodiodes, the data processing was done offline in two steps: in the first place, the acquired (raw) signals V_x and V_y were transformed into the processed error-corrected signals s_x and s_y (the arrow from Fig. 2(a) to Fig. 2(b)); this was followed by a phase-unwrapping transformation (the arrow from Fig. 2(b) to Fig. 2(c)).

In the first step we applied a correcting transformation fixing the slight $V(I)$ nonlinearities of both photodiodes. The signals were then low-pass filtered, thereby eliminating the unwanted high-frequency noise with an adjustable cutoff. The filtered signals were later separately normalized according to the maximum and minimum filtered voltage in each channel and shifted to eliminate the offsets. This procedure can be expanded to the case when the amplitudes $V_{x0,y0}$ and the zero offsets $V_{xoff,yoff}$ vary with time, which cannot be done with the standard least-squares fitting methods [10,13,14]. When the displacement is smaller than $\lambda/2$, the intensity extremes may not be reached, so in this case the raw signals have to be normalized and zero-shifted with the values of the extremes obtained before the real measurement is performed. The lack-of-quadrature correction was carried out last; it was derived from the work of Heydemann [10] and will be described in detail in subsection 3.1. After this software-based procedure, we obtained the processed error-corrected signals (Fig. 2(b)):

$$s_x(t) = \cos\delta(t) \quad \text{and} \quad s_y(t) = \sin\delta(t).$$

A Lissajous circle is obtained (Fig. 2(d)) by plotting the vector $(s_x(t), s_y(t))$. One revolution of the rotating vector path corresponds to a phase change of 2π. This is equivalent to a displacement by $\lambda/2$ of the measuring surface, so the measurement of the displacement becomes possible by following the phase of the rotating vector. As the measuring surface moves forward (towards the BS), the vector rotates in the counterclockwise direction. If it moves backward (away from the BS), the vector rotates in the clockwise direction.
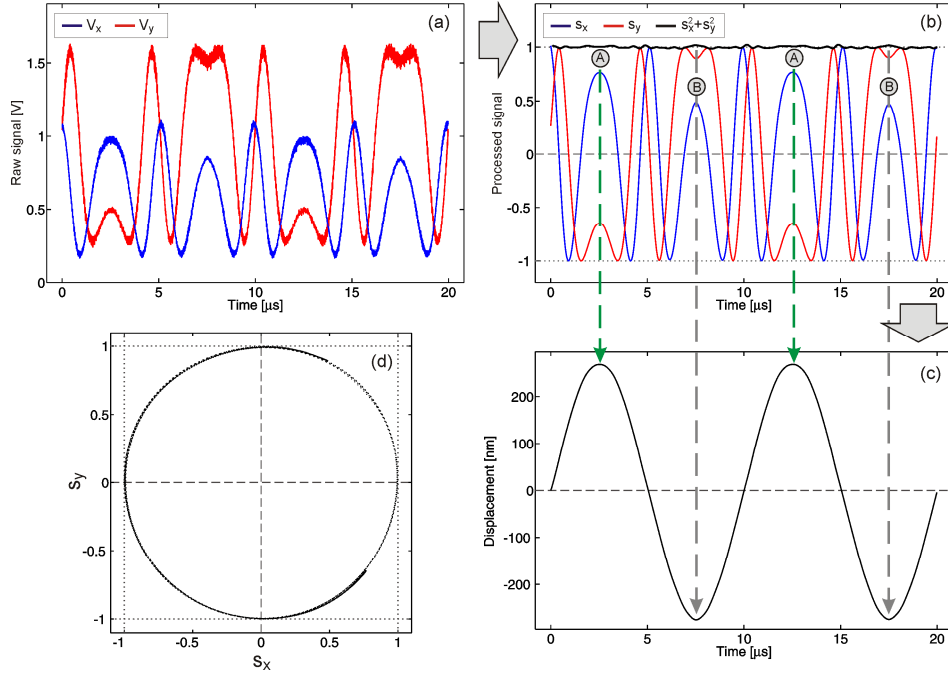
Fig. 2. The data processing of the two photodiode signals in the HQLI measurement of the harmonically vibrating mirror ($f = 100$ Hz, $A = 270$ nm) mounted on a PZT. (a) Raw signals: $V_x(t)$ and $V_y(t)$. (b) Processed error-corrected signals: $s_x(t)$ and $s_y(t)$. (c) Displacement as a function of the time obtained after the unwrapping of the phase. (d) Lissajous figure of the processed data: $(s_x(t), s_y(t))$.

In the second step, the displacement (Fig. 2(c)) was determined from s_x and s_y using a phase-unwrapping algorithm depicted in the flowchart in Ref [12]. The transition from the forward to the backward motion corresponds to the two crests (or two troughs) of s_x and s_y (the dashed line A in Fig. 2). The opposite transition (the dashed line B in Fig. 2) corresponds to the alternating second derivatives of s_x and s_y.

3.1 Correction of the quadrature phase-shift error

Once the photodiodes' nonlinearities are corrected, the amplitudes are normalized ($V_{x0,y0} = 1$) and the zero offsets are set to null ($V_{xoff,yoff} = 0$), the only significant remaining error in Eq. (4) is the quadrature phase-shift error. Setting $\delta_x = 0$ and $\delta_y = \alpha$, the ideal signals s_x and s_y are distorted by the phase-shift error and can be described by

$$s_{xe} = \cos\delta = s_x \quad \text{and} \quad s_{ye} = \cos(\delta - \alpha) = s_x \cos\alpha + s_y \sin\alpha,$$

where s_{xe} and s_{ye} correspond to the preprocessed signals before the phase correction is made.

Figure 3 shows two measurements of the displacement of the harmonically vibrating mirror driven by a PZT. First, the reference measurement u_r (the black line) was obtained with an adjusted HQLI. Then we rotated the OWP to change the phase shift to $\alpha = 117°$. An inaccurate measurement u_m performed with a HQLI lacking the phase quadrature is shown as the red line in Fig. 3(a). Both measurements were made at the same frequency and displacement amplitude of the vibrating mirror ($f = 100$ Hz, $A = 270$ nm).

The signals that are obtained with the adjusted interferometer are in exact quadrature ($\alpha = 90°$) and form a Lissajous circle (the black dots in Fig. 3(c)), described by the equation $s_x^2 + s_y^2 = 1$. In the case of a misaligned HQLI lacking the phase quadrature, the circle is deformed into an ellipse-like curve (the red dots in Fig. 3(c)). However, we can determine the phase shift α and correct the signals of an inaccurate measurement (s_{xe} and s_{ye}) as follows.
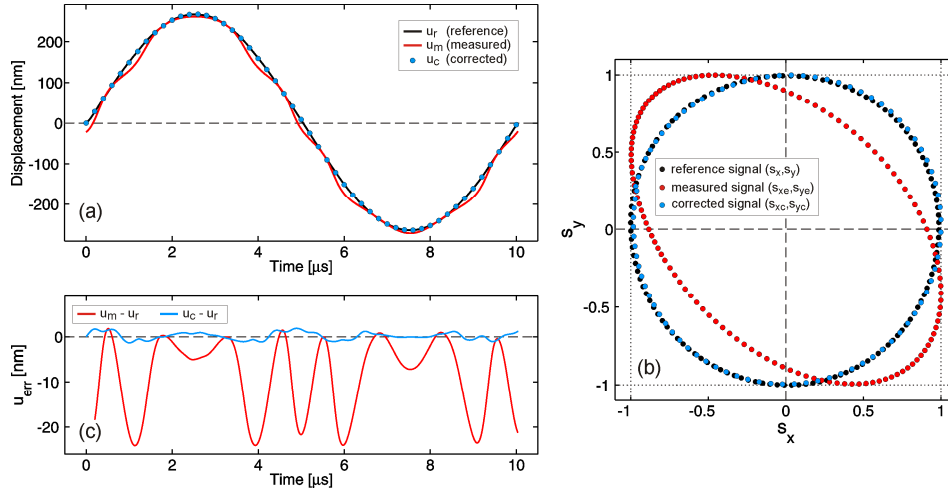
Fig. 3. The measured displacement of the harmonically vibrating mirror (f = 100 Hz, A = 270 nm). (a) Displacement as a function of time for the reference measurement u_r obtained with an adjusted HQMI (the black line), the inaccurate measurement u_m with a HQMI lacking the phase quadrature (the red line), and the software-corrected displacement u_c of the inaccurate measurement (the blue circles). (b) The Lissajous representation of the signals from which the displacements in (a) were derived. (c) The displacement error u_{err} between the distorted and the reference measurement $u_m - u_r$ (the red line) and the one between the software-corrected and the reference displacement $u_c - u_r$ (the blue line).

Substituting

$$s_x = s_{xe} \quad \text{and} \quad s_y = (s_{ye} - s_{xe} \cos \alpha) / \sin \alpha \tag{5}$$

into the equation of a circle we obtain the equation for an ellipse in the explicit form: $(s_{xe}^2 + s_{ye}^2) - 2 s_{xe} s_{ye} \cos \alpha = \sin^2 \alpha$. Since it is more convenient to fit an implicit function a suitable substitution needs to be applied to the equation of an ellipse. With $s_{xe} = r \cos \theta$ and $s_{ye} = r \sin \theta$, the ellipse is unwound to obtain the distance from the origin r as a function of the angle θ. The phase shift α is obtained by fitting the expression

$$r(\theta) = \sin \alpha \left(1 - \cos \alpha \sin 2\theta \right)^{-\frac{1}{2}}$$

to the transformed data pairs

$$\left(r = \sqrt{s_{xe}^2 + s_{ye}^2}, \theta = \arctan \frac{s_{ye}}{s_{xe}} \right)$$

using the method of least squares. Now that α has been determined by the fitting procedure the inaccurate data is corrected by inserting α back into Eqs. (5). Thus, the corrected signals s_{xc} and s_{yc} are obtained (the blue dots in Fig. 3(b)). The corrected displacement u_c (the blue dots in Fig. 3(a)) was calculated using the phase-unwrapping algorithm on the phase-shift-corrected data.

Figure 3(c) shows the displacement error between the inaccurate and the reference measurement $u_m - u_r$ (the red line) and the one between the software-corrected and the reference displacement $u_c - u_r$ (the blue line). The maximum displacement error was significantly reduced from the original 25 nm to the improved 3 nm. Moreover, the original error was periodic and severely unidirectional, while the corrected one is symmetrical around zero and without a period. Apart from the purpose of the software error correction, knowing

the phase shift between the signals also helps as a guide for the manual adjustment of the OWP angle φ.

The relation between the phase shift α and the angle of the OWP rotation φ is established from Eqs. (1) as

$$\alpha(\varphi) = \arctan(\cos 2\varphi - \sin 2\varphi) + \arctan(\cos 2\varphi + \sin 2\varphi). \qquad (6)$$

For the robust realization of a HQLI, a slight deviation from the adjusted angle of the OWP should not shift the phase significantly from the ideal 90°. The sensitivity of the phase shift on the OWP rotation corresponds to the slope $d\alpha/d\varphi$, which can be extracted from Eq. (6). In the ideal case, when the phase retardation between the two polarizations is achieved only through the OWP, the HQLI's accuracy is insensitive to slight variations of the OWP rotation. However, this may pose a problem if an additional phase shift originates from the polarization-sensitive light reflections, such as the reflection at the BS [17]. In the latter case, the OWP is used to add the remaining phase shift needed to achieve the phase quadrature, which may set the angle of the OWP rotation φ to the point where $d\alpha/d\varphi$ is large. This effect may, therefore, undermine the robustness of the interferometer and should be avoided.

4. Analysis of the quadrature phase-shift error

We carried out a detailed theoretical and experimental analysis of the displacement error originating from the lack of quadrature. The displacement error u_{err} is defined by subtracting the reference displacement u_r from the inaccurately measured one u_m as

$$u_{err}(\delta, \alpha) = u_m - u_r = \frac{\lambda}{4\pi}\left(\arctan\frac{s_{ye}}{s_{xe}} - \arctan\frac{s_y}{s_x}\right). \qquad (7)$$

We measured the displacement u_m of the measuring mirror, mounted on a PZT, at various angles of OWP rotation φ, i.e., for different phase shifts α (Eq. (6)). The PZT moved the mirror in two distinct modes: harmonic (e.g., the red line in Fig. 4(a)) and triangular (e.g., the red line in Fig. 4(b)). The mirror vibrating in harmonic mode had a frequency of 100 Hz and an amplitude of 270 nm. The triangular displacement's frequency and amplitude were 70 Hz and 330 nm, respectively. Using the above-described phase-correction algorithm we obtained the corrected displacement u_c (the black lines in Figs. 4(a) and 4(b)). The difference between the measured and corrected displacement $u_m - u_c$ is shown as a green line in Figs. 4(a) and 4(b). We assumed that this difference equals the displacement error defined in Eq. (6). The extremes of the error in Fig. 4(a) are shown as two circles in Fig. 4(c) at $\alpha = 43°$ and the error interval is indicated by "error H". Similarly, the two squares in Fig. 4(c) at $\alpha = 140°$ correspond to the error extremes of the triangular mode shown in Fig. 4(b). This error interval is indicated by "error T". The other circles and squares in Fig. 4(c) represent the error extremes of the displacement error obtained at various phase shifts for the harmonic and triangular modes, respectively.

Equation (6) shows that the rotation of the OWP produces the phase shift α in the interval between −90° and 90°. However, in our case the rotation of the OWP enabled measurements of the phase shift in the interval between −36° and 144°, because an additional phase shift of 54° originates from the polarization-sensitive light reflections at the BS. This phase shift was measured by removing the OWP from the HQLI. Its origin was proved by the BS rotation of 180° around the y-axis (see Fig. 1). After the rotation, the additional phase shift changed the sign, indicating that the BS was the only source of this shift. Due to this effect, the measured phase-shift interval in Fig. 4(c) exceeds 90°. When the phase shift is smaller than 10° it can no longer be determined, because of the extreme distortion of the Lissajous curve.

The shaded area in Fig. 4(c) displays the error region bounded by the theoretical lines u_{errB} and u_{errb} (the solid lines in Fig. 4(c)). To calculate the boundaries we need to find the extremes of Eq. (7) with respect to δ. Those that give an error which is further away from the zero error

are labeled δ_B, the others, which are closer to the zero error, are named δ_b. Substituting the locations of the extremes back into Eq. (7) gives the two bordering lines:

$$u_{errB}(\alpha) = u_{err}\left(\delta_B(\alpha), \alpha\right); \quad \text{where} \quad \delta_B(\alpha) = \frac{1}{2}\left(\alpha - \arccos\left(\frac{\sin\alpha - 1}{\cos\alpha}\right)\right), \quad (8a)$$

$$u_{errb}(\alpha) = u_{err}\left(\delta_b(\alpha), \alpha\right); \quad \text{where} \quad \delta_b(\alpha) = \frac{1}{2}\left(\alpha + \arccos\left(\frac{\sin\alpha - 1}{\cos\alpha}\right)\right). \quad (8b)$$

Equation (7) and Eqs. (8) represent a general theoretical result that depends only on the wavelength of the interferometric laser. It can also be applied to other quadrature-detection systems, such as optical encoders [6], where the constant $\lambda/(4\pi)$ in Eq. (7) is replaced by $p/(2\pi)$. Here, p is an arbitrary position period that equals $\lambda/2$ for the case of HQLI or λ/n for n-pass realizations of similar interferometers [12,19]. The results obtained with the HQLI can be generalized to other quadrature-detection systems, using the right-hand scale in Fig. 4(c). Additionally, the results are also valid when the quadrature-detection method is used to measure other quantities that change the optical phase difference.
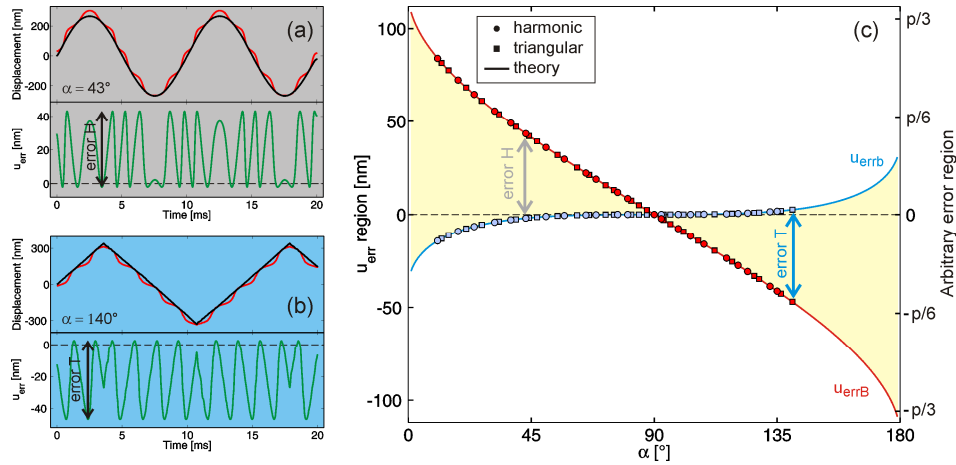

Fig. 4. The influence of the phase shift on the error in the displacement. (a) The reference ($\alpha = 90°$; the black line) and distorted ($\alpha = 43°$; the red line) harmonic displacements and the corresponding error marked as "error H". (b) The reference ($\alpha = 90°$; the black line) and distorted ($\alpha = 140°$; the red line) triangular displacements and the corresponding error marked as "error T". (c) The phase-shift displacement error u_{err} as a function of the phase shift α for $\lambda = 632.8$ nm (left scale) and the arbitrary position period p (right scale). The measured border errors of the harmonic ($f = 100$ Hz, $A = 270$ nm) and the triangular ($f = 70$ Hz, $A = 330$ nm) displacements for several values of α are marked as circles and squares. The theoretical error borders are calculated from Eqs. (8) (the blue and red lines).

Linearization of Eq. (7) by retaining the first non-zero term in the Taylor series expansion around $\alpha = 90°$ gives

$$\frac{\lambda}{4\pi}\left(90° - \alpha\right)\cos^2\delta$$

and indicates that the phase-shift displacement error is periodic with respect to δ. This two-cycle period, i.e., a periodicity of two-cycles as the difference in the optical path length changes from 0 to 2π, is $p/2$ (e.g., $\lambda/4$ for HQLI). The two-cycle period is seen in Figs. 3(a), 4(a) and 4(b).

Since the measured error extremes denoted by circles and squares perfectly match the theoretical curve, the assumption that $u_m - u_c = u_{err}$ is justified. The results presented in this

analysis show: (i) the error region is independent of the amplitude, the frequency and the shape of the displacement. It depends only on the laser wavelength or, in general, on the position period of quadrature-detection systems; (ii) the error is systematic, periodic and asymmetrical around the nominal displacement value; (iii) the described phase-shift correction algorithm significantly improves the accuracy, even for large deviations from the ideal phase quadrature. However, when the acquired signals lack the quadrature, the sensitivity of the HQLI is no longer constant. It is, therefore, necessary to adjust the interferometer close to the optimal 90° phase shift.

5. Conclusion

We have presented the theory and algorithms that make it possible for us to correct the typical errors that limit the precision and accuracy of displacement measurements performed with the HQLI. The errors arising from the lack of phase quadrature were analyzed in detail. The results obtained from the comparison between the measured and the reference displacements show that the presented phase-shift correction algorithm significantly improves the accuracy, even for the large deviations from an ideal phase quadrature.

The phase-shift error region was determined experimentally by comparing the measured and phase-shift error-corrected displacement. The results of the experimental assessment perfectly matched the theory, thus the described phase-shift correction algorithm is effective. The error arising from the lack of phase quadrature is systematic, has a two-cycle period, and is asymmetrical around the nominal displacement value, while the error region is independent of the amplitude, the frequency and the shape of the displacement.

The results of the quadrature phase-shift error analysis obtained with the HQLI can be applied to other quadrature-detection systems, even those which are not based on interferometry. In addition, these results are also valid when the quadrature-detection method is used to measure other quantities influencing the optical phase difference.